# Influence of Film Pressure Distribution on Leakage Stability of Mechanical Seal Faces

**Jing Wang[1,*], Zhonghua Zhou[2]**

[1] Chongqing Technology and Business Institute, Chongqing Open University, Chongqing 401520, China

[2] China Oilfield Services Limited, Sanhe 065200, Hebei, China

Corresponding Author: Jing Wang (1065560315@qq.com)

Funding: Scientific and Technological Research Project of Chongqing Municipal Education Commission (No. KJQN202204018): Research on Sealing Mechanism of Mechanical Equipment Lip Seal

**Abstract:** Mechanical seal is responsible for the control of media leakage in pumps, compressors and high-speed rotating equipment. The pressure distribution of the liquid film on the end face is directly related to the reliability of the equipment seal. Focusing on the influence of end-face membrane pressure distribution on leakage stability, this paper constructed CFD numerical simulation, finite element deformation calculation and sensor data calibration methods, solved the liquid film pressure field through the film lubrication equation, mapped the membrane pressure load to the finite element model, and analyzed the relationship between membrane pressure distribution and leakage fluctuation by combining pressure gradient extraction, low-pressure connected area identification and leakage fluctuation coefficient evaluation. Nine groups of rotation speed load experiments show that the average membrane pressure of the end face increases from 0.46 MPa to 1.18 MPa, the dispersion coefficient of membrane pressure increases from 0.083 to 0.214, the fluctuation coefficient of leakage increases from 0.061 to 0.186, and the correlation coefficient between them reaches 0.94. The research can provide technical basis for the optimization of mechanical seal end face structure and leakage risk control.

**Keywords:** Mechanical seal; End-mask pressure distribution; Leakage stability; CFD numerical simulation

## 1. Introduction

Mechanical seal is a key component to control media leakage in pumps, compressors and high-speed rotating equipment. The micrometer-level liquid film on the end face plays the role of lubrication, bearing and isolation, and its pressure distribution directly affects the shape of the leakage channel and the fluctuation of the leakage amount. In recent years, mechanical seal research has gradually shifted from empirical design to the combination of numerical simulation and experimental testing. Stanciu et al. used the finite element method to analyze the influence of fluid temperature on the leakage of mechanical seals, and pointed out that thermal deformation would change the end face clearance and leakage state [1]. Medjahed et al. simulated the gas encoiling process in the spiral groove mechanical seal and revealed the coupling relationship between the

groove structure and the flow field distribution [2]. Brunetiere et al. studied the behavior of pulse gas sealing through numerical simulation, which provided reference for the analysis of gas film pressure field [3]. Behadef et al. pointed out that the end face contact state and liquid film characteristics will jointly affect the operation stability [4]. Shevchenko constructed the closed design model of mechanical seal and emphasized the matching relationship between structural parameters and seal state [5]. The existing research provides a basis for the thermal deformation, flow field distribution and leakage test of the seal, but the analysis of the influence of the end-face pressure distribution on the leakage stability still needs to be deepened. Based on this, this paper uses CFD numerical simulation, finite element analysis and sensor data calibration methods to analyze the pressure field of liquid film, the change of film thickness and the evolution characteristics of leakage channel. The influence law of membrane pressure distribution on leakage stability is verified by rotational speed load experiment and membrane pressure fluctuation experiment.

### *2. Mechanical Seal End Mask Pressure Distribution and Leakage Stability Mechanism*

The liquid film on the end face of mechanical seal is under the joint action of rotational shear, axial closing force and medium pressure difference, and the membrane pressure distribution determines the carrying capacity of liquid film and the form of leakage channel [6]. When the end-face pressure decreases smoothly along the radial direction, the liquid film support is more balanced and the leakage fluctuation is small. When the local high-pressure area, low pressure area or circumferential pressure mutation appears, the film thickness will produce non-uniform change, and the low-pressure area is easy to form a continuous micro-leakage channel, which makes the leakage amount show periodic fluctuations. In order to characterize the leakage stability, the following evaluation indexes can be constructed:

$$S = \frac{\bar{Q}}{\sigma_Q + \varepsilon} \cdot \frac{\bar{P}}{P_{max} - P_{min} + \varepsilon} \tag{1}$$

Where, S is the leakage stability index, $\bar{Q}$ is the average leakage amount, $\sigma_Q$ is the standard deviation of leakage amount, $\bar{P}$ is the average membrane pressure, $P_{max}$ and $P_{min}$ are the maximum and minimum membrane pressure of the end face respectively, $\varepsilon$ is the correction constant to prevent the denominator from being zero. The larger this index is, the smoother the leakage process is.

## 3. Research Methods

### *3.1 Modeling Method of End-face Liquid Film Pressure Field Based on CFD Numerical Simulation*

The micro-gap between the dynamic ring and the static ring of the mechanical seal is taken as the computational domain for the pressure field modeling of the end-face liquid film, and the liquid film region is equivalent to the thin layer of rotating fluid space [7]. The model combines 3D geometric modeling with local mesh encryption, and sets pressure boundary, velocity boundary and non-slip boundary to the end surface inlet, outlet, rotating wall and static wall respectively. Considering that the thickness of the liquid film is much smaller than the radius of the end face, the fluid pressure distribution can be solved according to the film lubrication governing equation:

$$\frac{\partial}{\partial r}\left(\frac{rh^3}{12\mu}\frac{\partial p}{\partial r}\right) + \frac{1}{r}\frac{\partial}{\partial \theta}\left(\frac{h^3}{12\mu r}\frac{\partial p}{\partial \theta}\right) = \frac{\omega r}{2}\frac{\partial h}{\partial \theta} \tag{2}$$

Where $r$ is the radial coordinate, $\theta$ is the circumferential coordinate, $h$ is the liquid film thickness, $\mu$ is the dynamic viscosity of the medium, $p$ is the local film pressure, and $\omega$ is the

angular velocity. To further quantify the uniformity of membrane pressure distribution, the dispersion coefficient of membrane pressure is introduced as follows:

$$C_p = \frac{\sqrt{\frac{1}{n}\sum_{i=1}^{n}(p_i - \bar{p})^2}}{\bar{p}} \tag{3}$$

Where, $C_p$ is the dispersion coefficient of the membrane pressure, $p_i$ is the membrane pressure of the $i_{th}$ sampling node, $\bar{p}$ is the average membrane pressure of the end face, and n is the number of pressure sampling nodes. The index can be used to determine whether there is local concentration or mutation of the end face pressure, and provide a calculation basis for subsequent leakage stability analysis.

### *3.2 Calculation Method of Sealing End Face Deformation and Film Thickness Based on Finite Element Analysis*

After obtaining the liquid film pressure field of the end face, the membrane pressure distribution calculated by CFD is mapped to the finite element model of the sealing end face as a surface load, and the micro-deformation of the dynamic ring and static ring under the joint action of fluid pressure, closing force and support constraint is analyzed [8]. The finite element model is divided into annular end face solid elements, and the local mesh encryption is performed in the sealing contact area, so that the deformation changes in the pressure concentration area and the low-pressure expansion area can be accurately captured. The micro-deformation of the end face can be expressed as follows:

$$Ku = F_p + F_c \tag{4}$$

Where, $K$ is the stiffness matrix of the end face structure, $u$ is the node deformation displacement vector, $F_p$ is the membrane pressure load vector, $F_c$ is the external load vector formed by the closing force and assembly constraints. According to the normal deformation result of the joint, the actual film thickness of the end face can be further corrected:

$$h_j = h_0 + \Delta u_{s,j} - \Delta u_{r,j} \tag{5}$$

Where, $h_j$ is the corrected film thickness at the JTH node, $h_0$ is the initial liquid film thickness, $\Delta u_{s,j}$ is the normal deformation of the static ring end surface, and $\Delta u_{r,j}$ is the normal deformation of the dynamic ring end surface. The coupling relationship among membrane pressure-deformation-film thickness can be established by mapping the membrane pressure load, solving the end face deformation and calculating the film thickness inverse, which can provide the end face clearance data closer to the actual working condition for the subsequent leakage channel identification. Figure 1 shows the coupling calculation process between the membrane pressure, the deformation of the end face and the membrane thickness update of the sealing end face.

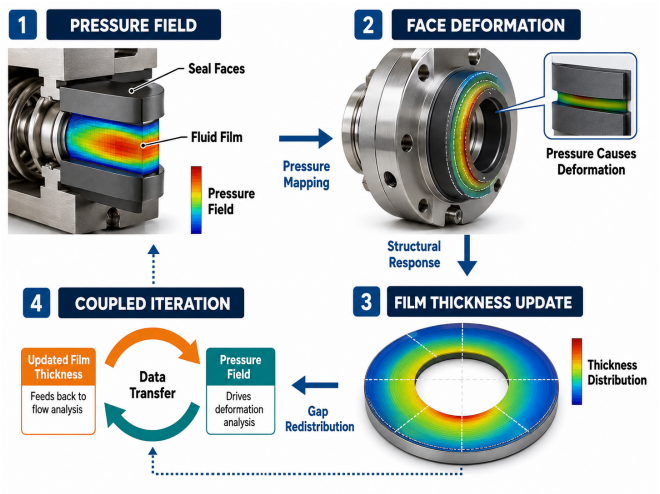


**Figure 1:** Schematic Diagram of Coupling Calculation of Pressure, Deformation and Thickness of Sealing end Mask.

### *3.3 Coupling Analysis Method of Pressure Gradient and Flow Field for Leakage Channel Identification*

Based on the calculated results of the end-face membrane pressure and thickness, the radial and circumferential pressure gradients of the sealing end-face were further extracted to identify low-pressure connected areas and potential leakage channels [9]. In the calculation process, the membrane pressure cloud map output by CFD is transformed into the node pressure matrix, and the local flow resistance change is judged by combining the film thickness distribution results. When the pressure gradient continuously increases in a certain area and the low membrane pressure area forms a connected relationship with the outlet boundary, it can be determined that there is a risk of leakage channel expansion in this area. The pressure gradient intensity can be expressed as follows:

$$G_{p,k} = \sqrt{\left(\frac{\partial p_k}{\partial r}\right)^2 + \left(\frac{1}{r}\frac{\partial p_k}{\partial \theta}\right)^2} \tag{6}$$

Where, $G_{p,k}$ is the pressure gradient strength of the KTH node, $p_k$ is the nodal membrane pressure, and r and $\theta$ are radial and circumferential coordinates, respectively. In order to quantify the risk of leakage channel, the proportion of low-voltage connected area is introduced as follows:

$$R_l = \frac{A_l}{A_s} \times 100\% \tag{7}$$

Where, $R_l$ is the proportion of low-pressure connected area, $A_l$ is the area that meets the low-pressure threshold and is connected with the outlet, $A_s$ is the effective liquid film area of the sealing end face. The higher this index is, the worse the continuity of the end surface liquid film support is, and the easier the leakage channel is formed. Through the calculation of pressure gradient, the segmentation of low-pressure area and the tracking of streamline, the location identification and risk judgment of the leakage channel can be realized. Figure 2 shows the specific process of leakage channel identification driven by pressure gradient.

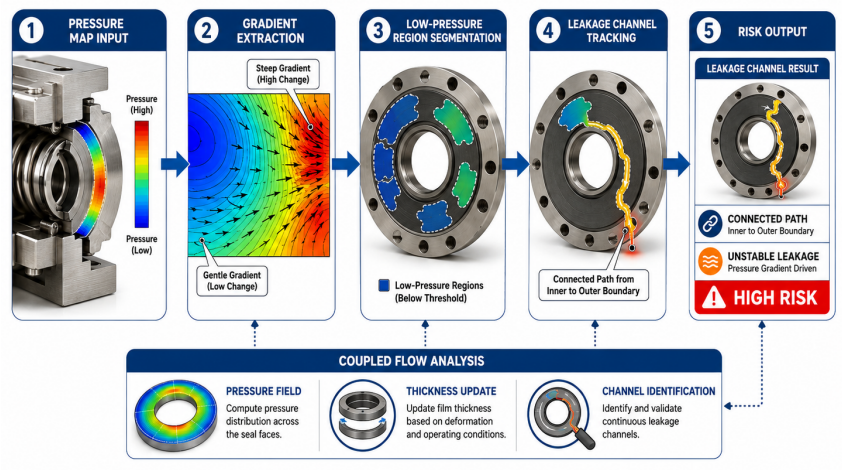


**Figure 2:** Flow Chart of Leakage Channel Identification Driven by Pressure Gradient.

3.4 Leakage Stability Evaluation Method Based on Calibration of Sensing Data

In order to improve the reliability of the leakage stability evaluation results, data collected by pressure sensors, flow sensors and temperature sensors are introduced into the numerical model calibration process in this paper. After abnormal point elimination, timestamp alignment and sliding window smoothing, the sensing data were compared with the membrane pressure distribution results obtained by CFD calculation to correct the boundary pressure, film thickness disturbance and leakage prediction deviation in the simulation model [10]. The sensing calibration error can be expressed as follows:

$$E_c = \frac{1}{m}\sum_{t=1}^{m}\left|\frac{Q_t^s - Q_t^c}{Q_t^s + \varepsilon}\right| \tag{8}$$

Where, $E_c$ is the sensing calibration error, $Q_t^s$ is the measured leakage at the TTH sampling time, $Q_t^c$ is the leakage calculated by simulation, m is the number of sampling points, ε is the correction constant. To further evaluate the stability of the leakage process, the leakage fluctuation coefficient is constructed as follows:

$$C_q = \frac{\sqrt{\frac{1}{m}\sum_{t=1}^{m}(Q_t^s - \bar{Q}^s)^2}}{\bar{Q}^s} \tag{9}$$

Where, $C_q$ is the leakage fluctuation coefficient and $\bar{Q}^s$ is the mean value of the measured leakage. The smaller this coefficient is, the more smoothly the leakage changes with time. Through the calibration of sensing data, the membrane pressure distribution, leakage fluctuation and working condition variation can be unified into the same evaluation framework, which provides a quantifiable basis for subsequent experimental verification.

## 4. Experimental Verification

In order to verify the influence of end mask pressure distribution on the leakage stability, this paper established a synchronous test platform for mechanical seal end mask pressure and leakage. The typical end contact mechanical seal assembly was selected as the experimental object, the medium was normal temperature water, the inlet pressure was set to 0.4MPa, 0.8MPa and 1.2MPa, and the speed was set to 1500 r/min, 3000 r/min and 4500 r/min to simulate the operation state under

different load and rotating shear conditions. During the experiment, the pressure change of the end face was collected by a miniature pressure sensor, the leakage per unit time was recorded by a flow sensor, and the temperature sensor was used to monitor the temperature rise of the medium near the end face to avoid large interference of temperature drift on the leakage results. Each group of working conditions was run continuously for 30 min, and the data of stable operation stage were taken for analysis, and the test was repeated for the same working condition three times to reduce accidental errors. After time synchronization, outliers' elimination and smoothing, the experimental data were compared with CFD simulation results and finite element film thickness calculation results. The corresponding relationship between the uniformity of film pressure distribution, the fluctuation amplitude of film pressure and the stability of leakage was mainly investigated.

### *4.1 End mask Pressure Distribution Experiment Under Different Speed Loading Conditions*

In order to analyze the influence of rotation speed and load changes on the distribution of end mask pressure, 9 groups of combined operating conditions were set up for testing. The rotational speeds were 1500 r/min, 3000 r/min and 4500 r/min, and the inlet pressures were 0.4 MPa, 0.8 MPa and 1.2 MPa, respectively. During the experiment, the pressure sensor arranges sampling points along the radial and circumferential direction of the end face, records the film pressure data during the stable operation stage, and calculates the average film pressure and the film pressure dispersion coefficient. The results show that with the increase of rotation speed and inlet pressure, the average membrane pressure of the end surface increases as a whole, and the carrying capacity of the liquid film increases. However, under the condition of high speed and high load, the phenomenon of local pressure concentration is more obvious, and the dispersion coefficient of membrane pressure increases synchronously, which indicates that the uniformity of pressure distribution on the end face decreases. This change will enlarge the gradient difference between the low-pressure area and the high-pressure area and provide inducing conditions for the subsequent leakage fluctuation. The experimental results are shown in Figure 3.

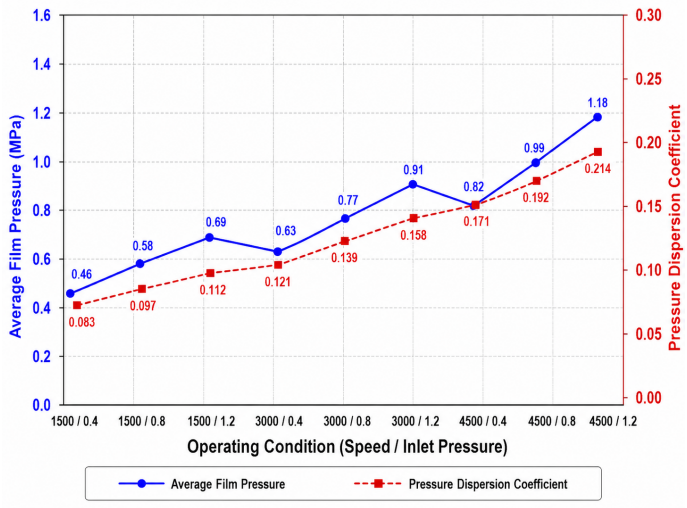


**Figure 3:** Change Curves of end Surface Average Membrane Pressure and Membrane Pressure Dispersion Coefficient Under Different Speed Loading Conditions.

As can be seen from Figure 3, when the inlet pressure increases from 0.4MPa to 1.2MPa and the

speed increases from 1500 r/min to 4500 r/min, the average membrane pressure of the end face increases from 0.46MPa to 1.18MPa, with an increase of about 156.5%. The dispersion coefficient of membrane pressure increased from 0.083 to 0.214, indicating that although the load level of membrane pressure distribution increased under high-speed load conditions, the uniformity decreased, and the local pressure mutation was more likely to induce leakage fluctuations.

### *4.2 Experiment on the Influence of Membrane Pressure Fluctuation on the Stability of Leakage*

In order to further analyze the influence of membrane pressure fluctuation on the stability of leakage, this paper selected 9 groups of membrane pressure fluctuation coefficient and leakage fluctuation coefficient under stable operation conditions for correlation analysis. In the experiment, the membrane pressure fluctuation coefficient was calculated by the end pressure sampling sequence, and the leakage fluctuation coefficient was calculated by the leakage change per unit time. The results show that when the film pressure fluctuation is small, the leakage changes smoothly. With the increase of the membrane pressure fluctuation coefficient, the discontinuous liquid film support is more likely to form in the local low-pressure area and the pressure mutation area of the end face, which leads to the intermittent expansion of the leakage channel and the leakage fluctuation. The relation curves between the fluctuation coefficient of membrane pressure and the fluctuation coefficient of leakage are shown in Figure 4.

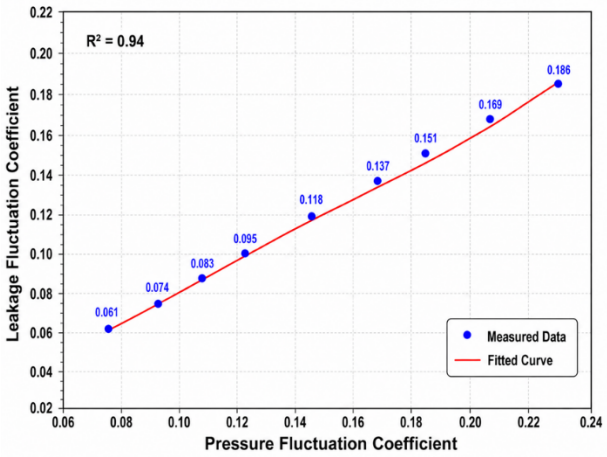


**Figure 4:** Curve of Relation Between Fluctuation Coefficient of Membrane Pressure and Fluctuation Coefficient of Leakage.

As can be seen from Figure 4, when the fluctuation coefficient of membrane pressure increases from 0.083 to 0.214, the fluctuation coefficient of leakage increases from 0.061 to 0.186. There is an obvious positive correlation between the two, and the fitting correlation coefficient reaches 0.94, indicating that the more uneven the distribution of membrane pressure, the worse the stability of leakage.

## 5. Conclusion

In this paper, an analysis process combining CFD pressure field solution, finite element film thickness correction, pressure gradient identification and sensor data calibration was established to solve the problem that the membrane pressure distribution at the end of the mechanical seal affects the leakage stability. The experimental results show that with the increase of rotation speed and inlet

pressure, the average membrane pressure on the end surface increases from 0.46 MPa to 1.18 MPa, and the dispersion coefficient of membrane pressure increases from 0.083 to 0.214, indicating that the local pressure concentration will weaken the uniformity of liquid film support. When the fluctuation coefficient of membrane pressure increases, the fluctuation coefficient of leakage increases from 0.061 to 0.186, and the correlation coefficient between them reaches 0.94, which verifies the influence of non-uniform distribution of membrane pressure on leakage stability. Subsequently, the temperature rise viscosity and wear evolution model can be combined to improve the accuracy of leakage prediction under complex working conditions.

**References**

[1] Stanciu A, Ripeanu R G. FEM Analyses on the Influence of Fluid Temperature on the Mechanical Seal Leakage. FME Transactions, 2025, 53(2): 212-224. DOI: 10.5937/fme2502212s.

[2] Medjahed A S, Blouin A, Pap B, Brunetière N. Simulation of Air Ingestion in a Mechanical Seal With Inward Pumping Spiral Grooves. Journal of Tribology, 2023, 145(11): 114401, 1-21. DOI: 10.1115/1.4062899.

[3] Brunetière N, Zahorulko A, Bouyer J. Numerical Simulation of the Behavior of Impulse Gas Seals. Tribology Online, 2024, 19(4): 360-366. DOI: 10.2474/trol.19.360.

[4] Behadef R, Gueraiche L. Friction Behavior of Conventional Mechanical Seals in Different Regimes. Journal of Bio- and Tribo-Corrosion, 2024, 10: 6. DOI: 10.1007/s40735-023-00810-4.

[5] Shevchenko S. Development of a Mechanical Seal Closed Design Model. IgMin Research, 2024, 2(2): 113-120. DOI: 10.61927/igmin152.

[6] Kuznetsov E, Pandová I. Calculation of the Operational Characteristics of the Impulse Gas-Barrier Face Seal. Management Systems in Production Engineering, 2023, 31(4): 411-417. DOI: 10.2478/mspe-2023-0046.

[7] Kuznetsov E, Panda A, Nahornyi V. Mathematical Model of the Working Process of an Impulse Type of Gas Barrier Face Seal. MM Science Journal, 2025, 2025(2): 8287-8291. DOI: 10.17973/MMSJ.2025_06_2025024.

[8] Fourt E, Arghir M, Jolly P, Andasmas M. Experimental Analysis of the Leakage Characteristics of Three Types of Annular Segmented Seals. Journal of Engineering for Gas Turbines and Power, 2023, 145(9): 091005. DOI: 10.1115/1.4062692.

[9] Jolly P, Arghir M, Kasahara H, Kimura W. Experimental Investigations on Carbon Segmented Seals With Smooth and Pocketed Pads. Journal of Engineering for Gas Turbines and Power, 2025, 147(6): 061014, 1-22. DOI: 10.1115/1.4066788.

[10] Badykov R, Falaleev S, Benedyuk M, Diligenskiy D. Dynamic Models of Mechanical Seals for Turbomachinery Application. Lubricants, 2024, 12(10): 355. DOI: 10.3390/lubricants12100355.